Contribution from the Departments of Chemistry, Dickinson College, Carlisle, Pennsylvania 17013, and University of Virginia, Charlottesville, Virginia 22901

Hypersensitivity in the Absorption Spectra of Erbium(III) Complexes in Aqueous Solution

SCOTT A. DAVIS*[1a] and F. S. RICHARDSON[1b]

Received April 20, 1983

Absorption spectra are reported for five different Er^{3+}/ligand systems in aqueous solution under variable pH conditions. The ligands differ with respect to their donor (ligating) atoms, their substituent groups. their chelation geometries, and their total coordination numbers. However, each includes two carboxylate groups in its structure. The absorption spectra of these systems are compared to that of $ErCl_3$/water over the 370–700-nm region, and oscillator strengths for the "hypersensitive" $^4I_{15/2} \rightarrow {}^2H_{11/2}$ and $^4G_{11/2}$ transitions of Er^{3+} are determined. Variations in these oscillator strengths with respect to ligand type and solution pH are rationalized in terms of ligand structure, ligand coordination properties, and ligand field geometry. Intensity calculations, based on a theoretical model for 4f → 4f electric dipole strengths, are carried out for a set of structures assumed to be similar to those of several of the complexes studied experimentally. The results of these calculations are compared to the observed intensity data and are discussed in terms of spectra–structure correlations in the $^4I_{15/2} \rightarrow {}^2H_{11/2}$ and $^4G_{11/2}$ hypersensitive transitions.

Introduction

The oscillator strengths of certain 4f → 4f transitions in lanthanide(III) complexes exhibit an especially strong sensitivity to the structural details and chemical nature of the ligand environment. This phenomenon is generally referred to as *hypersensitivity*, and it has been the subject of considerable experimental and theoretical investigation.[2-7] The hypersensitive transitions are of practical interest in lanthanide coordination chemistry because their spectral intensities can be used to probe complex formation, coordination geometry, ligand structure, and chelate–solvent interactions. Furthermore, since the absorption and emission intensities of these transitions can be dramatically modulated by ligand modification, they are of potential interest in the design of variable optical filters and phosphor materials. However, before these practical applications of lanthanide hypersensitivity can be fully realized, it is important that the underlying spectra–structure (ligand) relationships be reasonably well understood.

As a class, nearly all of the hypersensitive multiplet–multiplet (4f → 4f) transitions share a common set of selection rules at the intermediate-coupling level. These rules are just those of radiative electric quadrupolar processes for 4f → 4f transitions.[2-6] However, it is nearly certain that essentially all of the observed intensity in these transitions is dipolar in nature, with the major contributions coming from electric dipole mechanisms. An explanation for this can be found in the "inhomogeneous dielectric" theory of hypersensitivity proposed by Jorgensen and Judd[2] and in the "ligand polarization" model first proposed by Mason, Peacock, and Stewart.[3,4,8] Although formally dissimilar, these two theories of hypersensitivity are equivalent with respect to physical mechanisms. It is envisioned that the dipolar components of the radiation field induce a set of transient (electric) dipoles in the ligand environment that may couple to the 4f-electron distributions via electrostatic quadrupole (Ln)–dipole (ligand) interactions. In a noncentrosymmetric system, *or* a centrosymmetric system coupled to an odd number of *ungerade* phonon modes, these quadrupole-induced dipole interactions can lead to large amplifications of the 4f → 4f electric quadrupole transition probabilities.[9-11] Thus, the observed spectral transition is electric quadrupolar with respect to the 4f → 4f processes involved but is electric dipolar with respect to the overall radiation–molecule interaction processes. This accounts for the hypersensitive transitions often being referred to as "pseudoquadrupolar" in nature. Other theories and mechanisms of hypersensitivity have been proposed,[5] but none of these are as amenable to detailed theoretical analysis as the theory outlined above.

In the present paper we report absorption results obtained on a series of erbium(III) complexes in aqueous solution under variable pH conditions. Each of the ligands included in this study contains two terminal carboxylate groups (ensuring relatively strong Ln–ligand binding even at low pH), but these ligands differ from one another with respect to the remainder of their donor moieties and their nonligating substituent groups. The main objectives of the study were to determine if, and by how much, the 4f → 4f absorption spectra reflect differences in ligand coordination properties and structure and to correlate any observed spectral differences with specific structural parameters. To aid in the latter, intensity calculations based on a previously reported intensity model[7] were carried out. Of special interest are the absorption spectra obtained in the $^4I_{15/2} \rightarrow {}^2H_{11/2}$ and $^4I_{15/2} \rightarrow {}^4G_{11/2}$ transition regions of Er(III). These transitions are known to exhibit hypersensitive behavior,[4,5] and they satisfy electric quadrupole selection rules in the intermediate-coupling scheme.

The ligands included in this study were oxydiacetate (ODA), dipicolinate (DPA), iminodiacetate (IDA), (methylimino)diacetate (MIDA), and *N,N'*-ethylenebis(*N*-(*o*-hydroxyphenyl)glycine) (EHPG).[12] Both ODA and DPA are terdentate ligands that form pairs of coplanar (five-membered) chelate rings with a lanthanide ion.[13,14] The only difference between these two ligands is in the nature of their respective central donor moieties—an ether oxygen in ODA and a pyridyl group in DPA. The IDA and MIDA ligands are also potentially terdentate, but in these systems coplanarity of the chelate rings is precluded by the preferred sp^3 hybridization on the central nitrogen donor atoms.[15] The only difference between IDA and MIDA is the H vs. CH_3 substituent on the nitrogen

(1) (a) Dickinson College. (b) University of Virginia.
(2) Jorgensen, C. K.; Judd, B. R. *Mol. Phys.* **1964**, *8*, 281.
(3) Mason, S. F.; Peacock, R. D.; Stewart, B. *Mol. Phys.* **1975**, *30*, 1829.
(4) Peacock, R. D. *Struct. Bonding (Berlin)* **1975**, 22, 83.
(5) Henrie, D. E.; Fellows, R. L.; Choppin, G. R. *Coord. Chem. Rev.* **1976**, *18*, 199.
(6) Peacock, R. D. *Mol. Phys.* **1977**, *33*, 1239.
(7) Richardson, F. S.; Saxe, J. D.; Davis, S. A.; Faulkner, T. R. *Mol. Phys.* **1981**, *42*, 1401.
(8) Mason, S. F.; Peacock, R. D.; Stewart, B. *Chem. Phys. Lett.* **1974**, *29*, 149.
(9) Mason, S. F. *Struct. Bonding (Berlin)* **1980**, *39*, 43.
(10) Judd, B. R. *J. Chem. Phys.* **1979**, *70*, 4830.
(11) Faulkner, T. R.; Richardson, F. S. *Mol. Phys.* **1978**, *35*, 1141.
(12) The alternative, and more proper, name for EHPG is *N,N'*-bis(2-hydroxyphenyl)ethylenedinitrilo-*N,N'*-diacetate.
(13) Albertsson, J. *Acta Chem. Scand.* **1968**, *22*, 1563; *Ibid.* **1970**, *24*, 3527.
(14) Albertsson, J. *Acta Chem. Scand.* **1970**, *24*, 1213; *Ibid.* **1972**, *26*, 985, 1005, 1023.
(15) Oskarsson, A. *Acta Chem. Scand.* **1971**, *25*, 1206.

0020-1669/84/1323-0184$01.50/0

Table I. Experimentally Determined Oscillator Strengths for the $^4I_{15/2} \rightarrow {}^2H_{11/2}$ and $^4G_{11/2}$ Transitions under Three Different Solution pH Conditions

transition	ligand[a]	oscillator strength ($f/10^{-6}$) acidic[b]	neutral[c]	basic[d]
$^4I_{15/2} \rightarrow {}^2H_{11/2}$	ODA	5.1	5.2	5.7
	DPA	6.8	7.4	7.4
	IDA	3.7	5.6	5.9
	MIDA	3.6	6.0	6.9
	EHPG	4.8	17.1	17.4
$^4I_{15/2} \rightarrow {}^2G_{11/2}$	ODA	11.4	12.0	12.8
	DPA	13.9	14.8	14.8
	IDA	8.4	12.4	13.2
	MIDA	8.1	13.5	15.0
	EHPG	6.1	17.6	21.6

[a] For all ligands *except* EHPG, $[Er^{3+}]:[ligand] = 1:3$ with $[Er^{3+}] = 40$ mM. [b] pH ~3. [c] pH ~7. [d] 8 < pH < 10.

donor atom. The EHPG ligand is potentially hexadentate with two carboxylate donor moieties, two amino donor groups, and two phenolate donor moieties. However, for 1:1 Ln^{3+}:EHPG in aqueous solution, hexadentate chelation is not complete until pH >8.[16] We have, then, a set of ligands that differ with respect to their donor atoms, chelation modes, conformational properties, and substituent groups. It was expected that each of these structural differences will be reflected in the intensity behavior of the $^4I_{15/2} \rightarrow {}^2H_{11/2}$ and $^4I_{15/2} \rightarrow {}^4G_{11/2}$ hypersensitive transitions.

Experimental Section

$ErCl_3 \cdot 6H_2O$ (99.99%) was purchased from Aldrich and was used without further purification. Oxydiacetic acid ($ODAH_2$) and (methylimino)diacetic acid ($MIDAH_2$) were also purchased from Aldrich and used without further purification. Iminodiacetic acid ($IDAH_2$) and disodium dipicolinate ($DPANa_2$) were purchased from Sigma. *N,N'*-Ethylenebis(*N*-(*o*-hydroxyphenyl)glycine) (EHPG) was purchased from Pfaltz and Bauer and was purified and handled according to the procedures described in ref 16.

All spectroscopic measurements reported here were carried out on aqueous solution samples in which $[Er^{3+}] = 0.04$ M. For EHPG, $[Er^{3+}]:[ligand] = 1:1$. For all other ligands, $[Er^{3+}]:[ligand] = 1:3$. Solution pH adjustments were made by using dilute NH_4OH. Absorption spectra were recorded on a Cary 17D spectrophotometer with the samples contained in 2-cm quartz cells. Spectra were recorded over the 370–700-nm region.

Experimental Results

Eight multiplet-to-multiplet transitions occur within the 370–700-nm spectral region. These are $^4I_{15/2} \rightarrow {}^4G_{11/2}$, $^2H_{9/2}$, $^4F_{3/2}$, $^4F_{5/2}$, $^4F_{7/2}$, $^2H_{11/2}$, $^4S_{3/2}$, and $^4F_{9/2}$, given in order of *decreasing* transition frequencies. Among these transitions, the most intense are $^4I_{15/2} \rightarrow {}^4G_{11/2}$ (5.9×10^{-6}), $^4F_{7/2}$ (2.2×10^{-6}), $^2H_{11/2}$ (2.8×10^{-6}), and $^4F_{9/2}$ (2.4×10^{-6}), where the numbers in parentheses are transition oscillator strengths determined for $ErCl_3$ in aqueous solution. For the systems examined in this study, only the intensities of the $^4I_{15/2} \rightarrow {}^4G_{11/2}$ and $^2H_{11/2}$ transitions exhibited "hypersensitivity" to changes in the ligand environment about the Er^{3+} ions. In all cases, changes in the oscillator strengths of the $^4I_{15/2} \rightarrow {}^4F_{7/2}$ and $^4F_{9/2}$ transitions were found to be less than 25% of the values obtained for Er^{3+} (aq). However, these changes for the $^4I_{15/2} \rightarrow {}^4G_{11/2}$ and $^2H_{11/2}$ transitions were found to be as large as ~370% and ~620%, respectively. We shall focus our attention, therefore, on the results obtained for these latter transitions.

For each of the five Er^{3+}/ligand systems examined in this study, absorption spectra were recorded as a function of solution pH over the pH range 2.5–10.0 at intervals of 0.5–1.0 pH unit. Oscillator strengths determined for the $^4I_{15/2} \rightarrow {}^2H_{11/2}$ and $^4G_{11/2}$ transitions under three different solids pH conditions are listed in Table I for each of the systems studied. From the results in this table, we first note that the oscillator strengths observed for the Er^{3+}/ODA and Er^{3+}/DPA systems exhibit very little pH dependence. On the other hand, the oscillator strengths observed for the Er^{3+}/IDA, Er^{3+}/MIDA, and Er^{3+}/EHPG systems show large increases in going from pH 3 to pH 7 and then much smaller increases in going from pH 7 to pH 10. Plots of f vs. pH for Er^{3+}/IDA resemble titration curves with inflection points at pH ~4.2. Plots of f vs. pH for Er^{3+}/MIDA show an inflection point at pH ~5.0. Similar plots for Er^{3+}/EHPG show an inflection point at pH ~6.0. Ratios of f(complex)/f(aquo) under low pH and high pH solution conditions are given in Table II. An illustrated of spectral pH dependence is given in Figure 1.

Table II. Experimentally Determined f(complex)/f(aquo) Ratios for the $^4I_{15/2} \rightarrow {}^2H_{11/2}$ and $^4G_{11/2}$ Transitions

transition	ligand	f(complex)/f(aquo) low pH[a]	high pH[b]
$^4I_{15/2} \rightarrow {}^2H_{11/2}$	ODA	1.8	2.0
	DPA	2.4	2.6
	IDA	1.3	2.1
	MIDA	1.3	2.5
	EHPG	1.7	6.2
$^4I_{15/2} \rightarrow {}^4G_{11/2}$	ODA	1.9	2.2
	DPA	2.4	2.5
	IDA	1.4	2.2
	MIDA	1.4	2.5
	EHPG	1.1	3.7

[a] pH ~3. [b] pH 8-10.

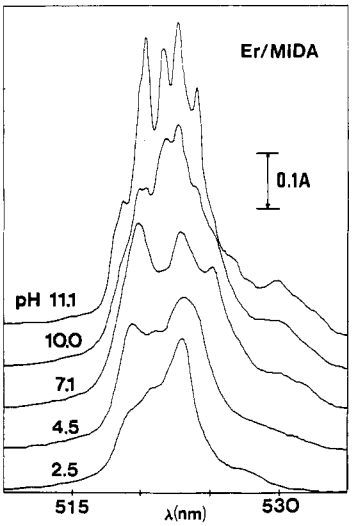

Figure 1. Absorption spectra in the $^4I_{15/2} \rightarrow {}^2H_{11/2}$ transition region for 1:3 Er^{3+}:MIDA in aqueous solution under different pH conditions.

The high-pH $^4I_{15/2} \rightarrow {}^4G_{11/2}$ spectra for Er^{3+}/ODA, -DPA, -IDA, and -MIDA are shown in Figure 2, and the high-pH $^4I_{15/2} \rightarrow {}^2H_{11/2}$ spectra for Er^{3+}/ODA and DPA are shown in Figure 4 (along with theoretically calculated spectra, vide infra).

Calculations

Energy level and intensity calculations were carried out for six different structures. Structure **1** has the formula ErL_9 and corresponds to a 9-coordinate Er^{3+}(aq) complex with D_{3h} point-group symmetry. Structure **2** has the formula ErL_8 and corresponds to an 8-coordinate Er^{3+}(aq) complex with D_{4d} point-group symmetry. ErL_9 (**1**) has a tricapped-trigonal-prism structure, and ErL_8 (**2**) has a bicapped-antiprism structure. In each case, L is intended to represent a water

(16) Salama, S.; Richardson, F. S. *Inorg. Chem.* **1980**, *19*, 635.

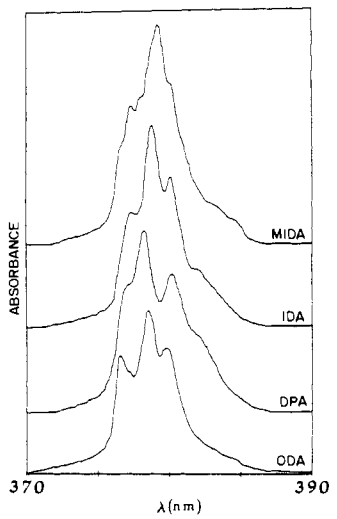

Figure 2. Comparison of absorption spectra in the $^4I_{15/2} \rightarrow {}^4G_{11/2}$ transition region for 1:3 Er^{3+}:ODA, Er^{3+}:DPA, Er^{3+}:IDA, and Er^{3+}:MIDA in aqueous solution at pH ~8.5.

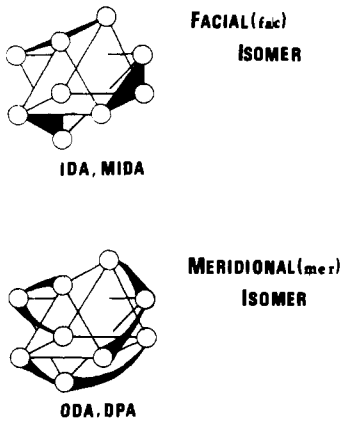

Figure 3. Coordination polyhedra associated with tris-terdentate binding of model ligands in solution.

molecule in a "united atom" approximation. Neither the coordination number nor the geometry of Er^{3+}(aq) complexes is known; however, our structures **1** and **2** represent the most likely idealized structures for these species.

Our structures **3** and **4** are the tris-terdentate $Er(ODA)_3^{3-}$ and $Er(DPA)_3^{3-}$ complexes, respectively. The coordination polyhedron in each of these structures forms a *distorted* tricapped trigonal prism with trigonal dihedral (D_3) symmetry. Carboxylate donor atoms form the top and bottom triangles of the prism, and the equatorial sites are occupied by the middle donor atoms of the respective ligands. In each case, the terdentate ligands stretch diagonally across the rectangular faces of the trigonal prism in the so-called meridional (*mer*) isomeric form (see Figure 15 of Favas and Kepert[17]). Our structures **3** and **4** correspond to those found for various $Ln(ODA)_3^{3-}$ and $Ln(DPA)_3^{3-}$ complexes in the solid state.[13,14] They also represent the most likely structures of the *majority* species in neutral-to-basic aqueous structures of 1:3 Er^{3+}:ODA and Er^{3+}:DPA.[18]

Our structures **5** and **6** are the tris-terdentate $Er(IDA)_3^{3-}$ and $Er(MIDA)_3^{3-}$ complexes, respectively. The coordination polyhedra in these structures are also of the tricapped-trigonal-prism form, but in these systems the ligands wrap around the prism in a facial (*fac*) isomeric configuration (see Figure 15 of Favas and Kepert[17]). The overall symmetry of structures

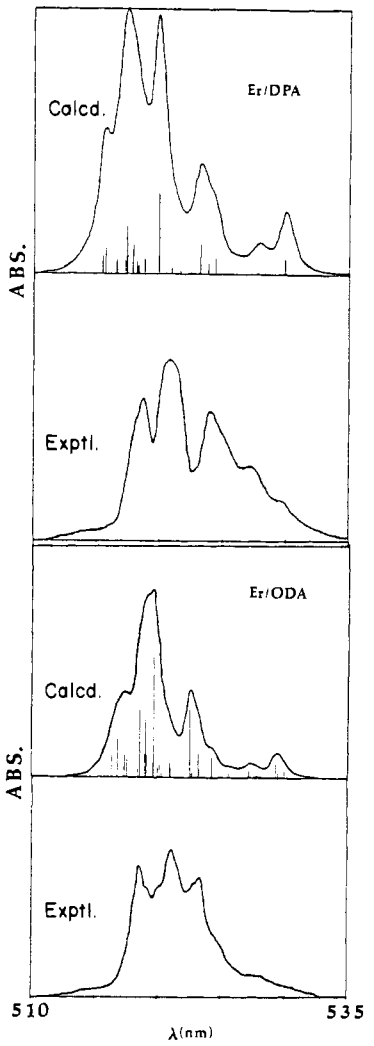

Figure 4. Calculated and observed absorption spectra in the $^4I_{15/2} \rightarrow {}^2H_{11/2}$ transition region for 1:3 Er^{3+}:ODA and Er^{3+}:DPA. The experimental spectra were obtained in aqueous solution at pH ~8.5. The calculated spectra are for structure **3** [$Er(ODA)_3^{3-}$] and structure **4** [$Er(DPA)_3^{3-}$].

5 and **6** is C_{3h}. It has been proposed that in neutral-to-basic aqueous solutions of 1:3 Ln^{3+}:IDA and Ln^{3+}:MIDA the *majority* of the species have structures similar to **5** and **6**.[18,19]

Our structures **3**–**6** have the following in common: (1) 9-fold coordination, (2) tricapped-trigonal-prism structures for the coordination polyhedra, (3) carboxylated donor atoms defining the top and bottom triangles of the trigonal prisms, and (4) "nearly" D_{3h} symmetry for the coordination polyhedra. Their differences are in (1) arrangement of the chelate rings about the lanthanide ion (**3** and **4** differ from **5** and **6** in this respect), (2) chelate ring conformations, and (3) the substituent groups attached to the middle donor atoms of the ligands. It is these differences that one may expect to be reflected in the absorption intensities of the hypersensitive transitions.

Energy Level Calculations. Crystal field wave functions and energy levels for the $4f^{11}$ electronic configuration of Er^{3+} are needed for carrying out electric dipole intensity calculations. These were obtained following the procedures reported in ref 7. The intermediate-coupling wave functions and multiplet baricenter energies were calculated by using a four-parameter "free-ion" Hamiltonian and a SLJ basis set comprised of all the Russell–Saunders states associated with the $4f^{11}$ configuration. The values of the four parameters (F_2, F_4, F_6, and ζ_{so})

(17) Favas, M. C.; Kepert, D. L. *Prog. Inorg. Chem.* **1981**, *28*, 309.
(18) Foster, D. R.; Richardson, F. S. *Inorg. Chem.*, in press.
(19) Salama, S.; Richardson, F. S. *J. Phys. Chem.* **1980**, *84*, 512.

Table III. Erbium(III) Electronic Parameters Used for Energy Level and Intensity Calculations[a]

F_2, cm^{-1}	433	$\Xi(1,2)$, cm^2 erg^{-1}	−0.57
F_4, cm^{-1}	67.2	$\Xi(3,2)$, cm^4 erg^{-1}	0.36
F_6, cm^{-1}	7.23	$\Xi(3,4)$, cm^4 erg^{-1}	0.37
$\langle r^2 \rangle$, Å^2	0.0466	$\Xi(5,4)$, cm^6 erg^{-1}	−0.44
$\langle r^4 \rangle$, Å^4	0.0759	$\Xi(5,6)$, cm^6 erg^{-1}	−0.92
$\langle r^6 \rangle$, Å^6	0.0969	$\Xi(7,6)$, cm^8 erg^{-1}	0.71
ζ_{SO}, cm^{-1}	2393		

[a] F_k denotes a Slater-Condon electrostatic radial parameter. ζ_{SO} denotes the radial spin-orbit coupling parameter. $\langle r^k \rangle$ denotes a 4f-electron radial expectation value, $\langle 4f|r^k|4f \rangle$. The $\Xi(t,\lambda)$ are *inter*configurational interaction parameters, as defined by Krupke.[21]

used in these calculations are listed in Table III.

The 4f-electron crystal field wave functions and energy levels were obtained by diagonalizing the appropriate crystal field Hamiltonian in a basis comprised of the 15 lowest energy intermediate-coupling states (multiplet levels). This basis was taken to be the same for all structures, and it included a total of 152 M_J levels. The parameters required in these calculations are the crystal field coefficients, $B_q^{(k)}$, of even parity (k = 2, 4, 6). These are defined by

$$H_{cf} = \sum_{k,q} B_q^{(k)} U_q^{(k)} \qquad (1)$$

where H_{cf} is the crystal field Hamiltonian and the $U_q^{(k)}$ are intraconfigurational unit tensor operators.[20] The $B_q^{(k)}$ coefficients are accessible to experimental determination *only* if one has spectra resolved at the crystal field level (i.e., spectra in which individual crystal field transitions can be resolved and assigned). This is not the case for our room-temperature solution-phase spectra, so we had to estimate the values of these coefficients from calculations based on the methods described in sections 2 and 3.4 of ref 7. These methods produce only rough estimates of the $B_q^{(k)}$ values, but they are based on a model of lanthanide–ligand interactions that is entirely consistent with our electric dipole intensity model for 4f → 4f transitions.[7] Quite accurate values of the $B_q^{(k)}$ coefficients would be required if our objective was to calculate distributions of electric dipole intensity among the crystal field components of multiplet-to-multiplet transitions (such as $^4I_{15/2} \rightarrow {}^2H_{11/2}$ and $^4G_{11/2}$). However, our more modest objective of calculating *overall* (or total) multiplet-to-multiplet transition strengths and intensities is much less demanding with regard to a detailed knowledge of the $B_q^{(k)}$ values.

The $B_q^{(k)}$ values used in all of the crystal field calculations reported here are listed in Table IV. Note that $B_6^{(6)}$ is a complex number for the C_{3h} crystal fields of structures **5** and **6**.

Transition Dipole Strengths. Electric and magnetic dipole transition strengths were calculated from precisely the same model and procedures described in ref 7. The radial parameters, $\langle r^k \rangle$, and interconfigurational interaction parameters, $\Xi(t,\lambda)$, required for calculating the electric dipole strengths are given in Table III. The $\Xi(t,\lambda)$ values are those of Krupke.[21] The values of $\langle r^k \rangle$ are the same as those used in our calculations of the $B_q^{(k)}$ coefficients. They are those given by Freeman and Watson[22] multiplied by a shielding factor ($1 - \sigma_k$). The values of the σ_k parameters were varied until the crystal field splittings within the $^4I_{15/2}$, $^2H_{11/2}$, and $^4G_{11/2}$ multiplets were compatible with the frequency ranges observed in the $^4I_{15/2} \rightarrow {}^2H_{11/2}$ and $^4I_{15/2} \rightarrow {}^4G_{11/2}$ absorption bands at room temperature. The final values used for the σ_k parameters were $\sigma_2 = 0.75$, $\sigma_4 = 0.14$, and $\sigma_6 = -0.11$.

Table IV. Even-Parity Crystal Field Coefficients (cm^{-1}) Used in Energy Level Calculations[a]

	structures					
$B_q^{(k)}$	1	2	3	4	5	6
$B_0^{(2)}$	323	213	−207	−261	−708	−680
$B_0^{(4)}$	−489	−386	−792	−894	186	214
$B_3^{(4)}$	*b*	*b*	−407	−385	*b*	*b*
$B_0^{(6)}$	−45.5	−86.2	127	94.4	294	302
$B_3^{(6)}$	*b*	*b*	111	115	*b*	*b*
$B_6^{(6)}$[c]	230	*b*	97.7	45.5	107 (9.99)	120 (7.00)

[a] Crystal field coefficients $B_q^{(k)}$ are defined according to eq 1. [b] These coefficients vanish by symmetry. [c] The $B_6^{(6)}$ coefficient has both real and imaginary parts in the C_{3h} symmetry of structures 5 and 6. The imaginary part is given in parentheses.

Three types of ligand parameters were required for our electric dipole strength calculations: (1) atomic (or perturber site) positional coordinates, (2) perturber site charges (q), and (3) perturber site dipolar polarizabilities ($\bar{\alpha}$), assumed to be isotropic in this study. The charge and polarizability parameters assigned to the ODA, DPA, IDA, and MIDA ligands are listed in Table V. Note that for DPA the polarizability of the pyridyl moiety is located at the centroid (of mass) of the pyridine ring. In our calculations on structures **1** and **2**, each of the water molecules was treated as a *point* perturber site with a charge of −0.3e and a polarizability of 1.49 Å^3.

The structure parameters for **1** and **3**–**6** were adapted from X-ray crystallographic data reported for similar systems.[13-15,23] Structure determinations have been reported for a number of $Ln(ODA)_3^{3-}$ and $Ln(DPA)_3^{3-}$ complexes,[13,14] so in these cases (structures **3** and **4**) only the Ln—O and Ln—N bond distances were modified to values appropriate for Ln = Er. $Ln(IDA)_3^{3-}$ and $Ln(MIDA)_3^{3-}$ complexes have not yet been isolated in the solid state. However, a crystal determination has been reported for the compound $Nd(IDA)Cl\cdot 3H_2O$.[15] The coordination polyhedron about each Nd^{3+} ion in this structure includes one terdentate Nd(IDA) chelate system. The ligand structure parameters of this system were used in constructing our structures **5** and **6**. Our structure **2** has an idealized geometry with the eight point ligands occupying sites located at the vertices of a bicapped-square anitprism (having exact D_{4d} symmetry). The Er-ligating distances used in each of our structures **1**–**6** are given in Table VI.

All of the calculated results reported here were obtained with use of the electronic and structural parameters listed in Tables III–VI and described above. A few additional calculations involving some parameter variations were carried out, but no attempt was made to "optimize" our choice of parameter values to match experimental observation. The latter could not be justified given the approximations inherent to our model and the uncertainties regarding the actual structures of the complexes in solution.

There are three types of contributors to the electric dipole strengths calculated according to the model employed in the present study.[7,24] These are the static-coupling ($D^{(s)}$), dynamic-coupling ($D^{(d)}$), and static/dynamic-coupling cross-term ($D^{(s,d)}$) contributors. The mechanisms underlying each of these contributors have been discussed elsewhere.[7,24] The static-coupling contributions are related to the original Judd–Ofelt theory of 4f → 4f electric dipole intensities,[25,26] the dynamic-coupling contributions are related to the Mason–Peacock "ligand polarization" model,[3,4,8,9] and the cross-term contributions arise from interference effects between the static-

(20) Hufner, S. "Optical Spectra of Transparent Rare Earth Compounds"; Academic Press: New York, 1978.
(21) Krupke, W. F. *Phys. Rev.* **1966**, *145*, 325.
(22) Freeman, A. J.; Watson, R. E. *Phys. Rev.* **1962**, *127*, 2058.
(23) Helmholtz, L. *J. Am. Chem. Soc.* **1939**, *61*, 1544.
(24) Richardson, F. S. *Chem. Phys. Lett.* **1982**, *86*, 47.
(25) Judd, B. R. *Phys. Rev.* **1962**, *127*, 750.
(26) Ofelt, G. S. *J. Chem. Phys.* **1962**, *37*, 54.

Table V. Charge (q) and Polarizability ($\bar{\alpha}$) Parameters Assigned to the ODA, DPA, IDA, and MIDA Ligands

	ODA		DPA		IDA		MIDA	
site[a]	q, e	$\bar{\alpha}$, Å^3	q, e	$\bar{\alpha}$, Å^3	q, e	$\bar{\alpha}$, Å^3	q, e	$\bar{\alpha}$, Å^3
O(1)*	0.20−	0.65						
O(2)*	1.15−	0.91	1.15−	0.91	1.15−	0.91	1.15−	0.91
O(3)	0.44−	0.84	0.44−	0.84	0.44−	0.84	0.44−	0.84
C(1)	0.09+	1.03			0.04+	1.03	0.09+	1.03
C(2)	0.57+	1.03	0.57+	1.03	0.57+	1.03	0.57+	1.03
N(1)*			0.15−	0	0.20−	1.03	0.15−	1.19
H(1)	0.08+	0.41			0.08+	0.41	0.08+	0.41
H(N)					0.08+	0.41		
Me(N)							0.09+	1.03
Py				10.0				

[a] Atoms are defined as follows: O(1), ether oxygen atom in ODA; O(2), coordinated oxygen atom of the carboxylate group; O(3), uncoordinated oxygen atom of the carboxylate group; C(1), methylene carbon atom; N(1), nitrogen donor atom in DPA, IDA, and MIDA; H(1), methylene hydrogen atom; Me(N), methyl substituent in MIDA; Py, centroid of the pyridyl moiety in DPA. Asterisks denote ligating atoms.

Table VI. Er–Ligating Atom Distances (Å) for Structures 1–6

	structures					
Er–L bond[a]	1	2	3	4	5	6
Er–O(H_2O)	2.45	2.45				
Er–O(1)			2.49			
Er–O(2)			2.40	2.40	2.47	2.47
Er–N(1)				2.47	2.51	2.51

[a] See Table V for numbering of ligand atoms.

Table VII. Electric Dipole Strengths Calculated for the $^4I_{15/2} \rightarrow {}^2H_{11/2}$ and $^4I_{15/2} \rightarrow {}^4G_{11/2}$ Transitions of Structures 1–6

		elec dipole strength,[a] 10^{-6} D^2			
transition	structure	$D^{(s)}$	$D^{(d)}$	$D^{(s,d)}$	D(total)
$^4I_{15/2} \rightarrow {}^2H_{11/2}$	1	33.4	3.61	−2.50	34.5
	2	12.1	1.02	4.11	17.2
	3	666	15.8	94.5	776
	4	674	79.3	219	972
	5	212	283	167	662
	6	221	364	216	801
$^4I_{15/2} \rightarrow {}^4G_{11/2}$	1	43.9	4.76	−2.70	46.0
	2	14.3	1.62	5.06	21.0
	3	904	21.1	127	1050
	4	917	106	296	1320
	5	250	379	245	874
	6	265	489	310	1064

[a] $D^{(s)}$ = static-coupling contributions, $D^{(d)}$ = dynamic-coupling contribution, $D^{(s,d)}$ = static/dynamic-coupling cross-term contribution, and D(total) = $D^{(s)} + D^{(d)} + D^{(s,d)}$.

coupling and dynamic-coupling transition moments.[24] Among the parameters introduced in our model, $D^{(s)}$ depends upon the $\Xi(t,\lambda)$ and ligand charge (q) parameters, $D^{(d)}$ depends on the $\langle r^k \rangle$ and ligand polarizability ($\bar{\alpha}$) parameters, and $D^{(s,d)}$ depends on all four of these parameter sets. Each of the dipole strength contributions exhibits a different dependence on ligand geometry.

Calculated Results. Electric dipole strengths for the $^4I_{15/2} \rightarrow {}^2H_{11/2}$ and $^4G_{11/2}$ transitions of structures **1–6** are given in Table VII. The numbers in this table were calculated assuming a $2J + 1$ (16-fold) degeneracy in the $^4I_{15/2}$ multiplet (i.e., they do *not* reflect a Boltzmann equilibrium distribution among the crystal field levels of $^4I_{15/2}$). For all structures, the magnetic dipole strengths calculated for these transitions were found to be *at least* 2 orders of magnitude smaller than the electric dipole strengths. Of special note among the results shown in Table VII are the following: (1) the small $D^{(d)}$:$D^{(s)}$ ratios calculated for structures **3** and **4**, (2) the relatively large $D^{(d)}$:$D^{(s)}$ ratios calculated for structures **5** and **6**, and (3) the significant $D^{(s,d)}$ contributions calculated for structures **4–6**. On the basis of ligand polarizability alone, one might expect **4** to have the largest $D^{(d)}$:$D^{(s)}$ ratios and **3**, **5**, and **6** to have

Table VIII. Comparison of Calculated vs. Experimentally Measured Oscillator Strengths

	calcd		exptl[a]	
transition	structure	$f/10^{-6}$	ligand	$f/10^{-6}$
$^4I_{15/2} \rightarrow {}^2H_{11/2}$	1	0.32	H_2O	2.8
	2	0.16		
	3	7.06	ODA	5.7
	4	8.83	DPA	7.4
	5	6.02	IDA	5.9
	6	7.28	MIDA	6.9
$^4I_{15/2} \rightarrow {}^4G_{11/2}$	1	0.58	H_2O	5.9
	2	0.26		
	3	13.2	ODA	12.8
	4	16.6	DPA	14.8
	5	11.1	IDA	13.2
	6	13.4	MIDA	15.0

[a] From spectra obtained on solutions with $8 < pH < 10$.

$D^{(d)}$:$D^{(s)}$ ratios of approximately the same magnitude. The differences between **3** and **4** vs. **5** and **6** indicate that the $D^{(d)}$:$D^{(s)}$ ratios are, in these cases, more sensitive to geometrical factors than to ligand charge and polarizability. (Recall that **3** and **4** have D_3 symmetry and planar terdentate chelate systems, whereas **5** and **6** have C_{3h} symmetry and nonplanar terdentate chelate systems.) The $D^{(d)}$:$D^{(s)}$ ratios appear to be very sensitive to the distribution of chelate rings about the lanthanide ion.

Our structures **1** and **2** were intended to mimic the most likely $Er(H_2O)_n^{3+}$ complexes present in aqueous solutions of $ErCl_3$. Similarly, our structures **3** and **4** were intended to mimic the majority species present in aqueous solutions of 1:3 Er^{3+}:ODA and 1:3 Er^{3+}:DPA at pH >7. Finally, our structures **5** and **6** were intended to mimic the majority species present in aqueous solutions of 1:3 Er^{3+}:IDA and 1:3 Er^{3+}:MIDA at pH >8. With these correlations in mind, we present Table VIII, which lists calculated and observed oscillator strengths for the various structures. The most striking aspects of the data shown in this table are (1) the remarkably good agreement between the oscillator strengths calculated for structures **3–6** and those observed for the corresponding 1:3 Er^{3+}:ligand systems and (2) our underestimate of the Er^{3+}(aq) oscillator strengths by about 1 order of magnitude. The latter can possibly be rationalized on the basis of our neglect of anion effects, $Er(H_2O)_n^{3+}$---Cl^- interactions, on the Er^{3+} spectra. These interactions would be expected to exist and to reduce the "effective" symmetry of the ligand environment sensed by the Er^{3+} ions. Furthermore, given the relatively large polarizability of Cl^- ions, one would predict that such interactions would enhance 4f → 4f electric dipole intensity via the dynamic-coupling (or ligand polarization) mechanism. Anion effects on the spectra of the various 1:3 Er^{3+}:ligand systems

would be expected to be significantly smaller, since in these systems the large organic ligands would effectively "insulate" the Er^{3+} ions from outer-sphere perturbations.

The correlations suggested by Table VIII must be considered with a great deal of circumspection. Our intensity model and parameterization schemes are much too approximate to legitimatize the good agreement achieved between theory and experiment. Furthermore, our structure models, especially for IDA (**5**) and MIDA (**6**), are highly idealized and do not reflect all of the complex species certain to be present in solution (even at pH >7). However, even with these qualifying remarks, the results obtained in this study suggest that the intensity model has considerable merit for rationalizing 4f → 4f intensity data.

One final comparison between our calculated and observed intensity data can be found in Figure 4. In this figure, calculated spectra are shown for structures **3** and **4** along with obseved spectra for 1:3 Er^{3+}:ODA and Er^{3+}:DPA at pH ~8.5. The vertical bars in the calculated spectra represent *Boltzmann-weighted* oscillator strengths (T = 298 K) computed for individual crystal field transitions within the $^4I_{15/2} \rightarrow {}^2H_{11/2}$ manifold. The solid line traces were calculated by giving each crystal field line a Lorentzian band shape and then summing over all the crystal field components of $^4I_{15/2} \rightarrow {}^2H_{11/2}$. The energy spacings between the crystal field levels of $^4I_{15/2}$ were taken directly from the crystal field calculations described earlier in this section.

Discussion

The low-pH results given in Table II indicate Er^{3+}–carboxylate coordination for all of the systems at pH 3. That is, in each case f(complex)/f(aquo) > 1. The relatively larger values of this ratio observed for the ODA and DPA systems vs. the IDA and MIDA systems can, most likely, be attributed to ligand conformational effects on chelation behavior. Bidentate chelation via the COO^- groups on ODA and DPA would force the *middle* (weaker) donor atoms into the inner coordination sphere of the Er^{3+} ion, expelling three water molecules for each ODA or DPA ligand that is bound. On the other hand, bidentate chelation via the COO^- groups in IDA and MIDA does *not* require that the middle (N) donor atoms enter the inner coordination sphere.

The relatively small increases of f(complex)/f(aquo) observed for ODA and DPA in going from low pH to high pH can be attributed primarily to changes in the relative concentrations of the various $Er(ODA)_n^{3-2n}$ and $Er(DPA)_n^{3-2n}$ species (n = 1–3) present in solution. The much larger increases observed for the IDA and MIDA systems, especially in the pH 4–6 range, can be attributed primarily to Er–N coordination and the formation of terdentate chelate systems. By far the largest low-pH to high-pH changes in the f(complex)/f(aquo) are observed for the 1:1 Er^{3+}:EHPG system. These changes are most dramatic over the pH 5–7 range. This is the pH range over which the two phenolic groups of the ligand are being deprotonated.[16] It has been proposed in the case of 1:1 Tb^{3+}:EHPG that by pH 7 the ligand is hexacoordinated to the lanthanide ion via two carboxylate groups, two amino groups, and two phenolate groups.[16] It is reasonable to assume that 1:1 Er^{3+}:EHPG would exhibit similar coordination properties. Hexacoordination (involving five chelate rings) and the presence of four negatively charged donor groups and two highly polarizable ligand moieties (the phenolate groups) give Er^{3+}/EHPG many of the structural features thought to be important to 4f → 4f electric dipole intensity enhancement. Since the largest increases in f(complex)/f(aquo) occur over the pH region in which the phenolate groups are entering the coordination sphere, it is tempting to associate these increases with ligand polarization effects, such as those envisioned by Mason and Peacock in their theory of hypersensitivity.[3,4] However, some caution must be exercised in this regard since it is certain that the geometry and "effective" symmetry of the ligand field about the lanthanide ion are also changing over this pH region, with respect to *both* the ligand charge and polarizability distribution. It may be that the observed intensity changes are due more to changes in ligand field geometry than to changes in ligand polarizability.

The remarkably good agreement between the calculated and observed oscillator strength values listed in Table VIII (excepting those for structures **1** and **2** and Er^{3+}(aq)) should not be taken either as a confirmation of the validity of our intensity model or as proof for the high-pH structures of the various Er^{3+}/ligand systems in aqueous solution. In both these respects, the results are encouraging and suggestive, but far from conclusive. The most interesting theoretical results obtained in this study are those showing the structural dependence of the relative $D^{(s)}$ vs. $D^{(d)}$ vs. $D^{(s,d)}$ contributions to electric dipole strength (see Table VII). For any *given* structure, the $D^{(s)}$:$D^{(d)}$:$D^{(s,d)}$ ratios can be changed quantitatively by making changes in the values adopted for the electronic parameters, $\langle r^k \rangle$, and $\Xi(t,\lambda)$ and the ligand parameters, q and $\bar{\alpha}$. However, for any "reasonable" changes made in the values of these parameters, the same qualitative results are obtained. That is, structures **3** and **4** always give $D^{(s)}$:$D^{(d)}$ ratios >>1, whereas structures **5** and **6** give $D^{(s)}$:$D^{(d)}$ ratios <1. Within the context of our intensity model, this is clearly a geometry-related effect rather than a ligand charge or polarizability effect. The calculated results given in Table VII also suggest that caution should be exercised in any attempt to relate hypersensitivity *exclusively* to either ligand polarization (dynamic-coupling) effects or crystal field point-charge (static-coupling) effects. Although this point is generally appreciated, its consideration is often abandoned in analysis of intensity data showing hypersensitivity.

Acknowledgment. This work was supported by the National Science Foundation (NSF Grant CHE80-04209 to F.S.R.).